Jurnal Ilmiah KURSOR
Menuju Solusi Teknologi Informasi
Vol. 12, No. 3, Juli 2024

ISSN 0216 – 0544
e-ISSN 2301– 6914

MULTIPLE BRAIN TUMOR WITH MODIFIED DENSENET121 ARCHITECTURE USING BRAIN MRI IMAGES

[a] Syaqila Sal Sabila, [b*] Hapsari Peni Agustin Tjahyaningtyas

[a,b] Department of Electrical Engineering, Universitas Negeri Surabaya
E-mail: syaqilasal.20040@mhs.unesa.ac.id, *hapsaripeni@unesa.ac.id

Abstract

Brain tumors are capable of developing in individuals of all ages and can originate from brain tissue in various shapes and sizes. As a result, it is critical to quickly identify patients in order to expedite treatment. Magnetic Resonance Imaging (MRI) of the brain is an appropriate technique for identifying chronic conditions, including tumors. Deep learning methodologies have suggested numerous medical analysis strategies for health monitoring and brain tumor identification. This study used a modified version of DenseNet121 to accurately categorize three different forms of brain tumors: meningioma, pituitary, and glioma. Following the last transition layer, the DenseNet121 modification adds DropOut and GlobalAveragePooling layers. We determine the optimal hyperparameters that yield the highest performance by comparing several factors, including dropout, epoch, optimizer, and activation function. Evaluation of classification performance involves a comparison between Basic CNN and Basic DenseNet. Results of the analysis show that the modified DenseNet121 model works best with the following ideal hyperparameters: ADAM optimizer, Softmax activation, 150 epochs of training, and an 0.8 dropout rate. The performance results show an accuracy value of 0.9782, exceeding previous research findings.

Key words: Brain Tumor, Classification, CNN, DenseNet121, MRI.

INTRODUCTION

Brain tumors are distinguished by the uncontrolled and aberrant proliferation of cells in brain tissue, which results in the disruption of normal brain function [1]. Brain tumors can develop in people of every age and can originate in brain tissue, presenting a diverse array of shapes and sizes. Brain malignancies are divided into two categories according to their original site: primary tumors and secondary malignancies [2]. Primary tumors arise within the brain tissue, whereas secondary malignancies metastasize from other regions of the body and enter the brain tissue via the circulation [3]. Malignant brain tumors, including glioma and meningioma, can be fatal if not detected in their early phases [4]. The World Health Organization (WHO) classifies brain tumors into four distinct groups. The Global Cancer Observatory recorded around 308,162 cases of brain tumors worldwide in 2020. The data shows that Asia has the highest occurrence rate, namely at 54.2% [5].

Based on the information provided, it is crucial to promptly diagnose people who are contaminated. Brain tumors are believed to be more effectively detected by MRI [6]. Brain tumors are composed of soft tissue and can only be detected with the use of an MRI scan [7]. MRI scans are highly sensitive and provide detailed picture information, enabling them to differentiate between soft and hard tissue in the brain [8] [9].

In the process of diagnosing brain tumors, clinicians frequently employ biopsies and physical observations as diagnostic procedures [10]. Although the manual method is error-prone, the biopsy procedure (including laboratory testing) takes around 10-15 days [11]. Alternative approaches with a reduced error rate and decreased processing time are necessary to aid physicians in their decision-making. Computer-aided Diagnosis (CAD) enhances the precision of patient diagnosis, leading to improved early detection and ultimately enhancing the patient's quality of life [12] [13].

Using a technique for categorizing brain malignancies on MRI images, CAD-assisted brain tumor diagnosis is presently being implemented. Machine Learning (ML) is an often employed technique. In 2017, Vani et al. employed the Support Vector Machine (SVM) method to categorize brain cancers into two categories: tumors present and tumors absent, achieving a 80% accuracy [14]. The researchers in Zaw's study investigated the efficacy of decision tree and naïve Bayes algorithms in the classification of brain tumors. The classification findings demonstrate that decision trees provide superior performance compared to naïve Bayes, with an accuracy of 94% [15]. Despite the remarkable efficacy of machine learning methods, including classification, in numerous applications, several drawbacks must be taken into account, one of which is the labor-intensive process of feature extraction that must be performed manually [16]. In order to create the most effective features, it is necessary to do research on different combinations of features.

A Convolutional Neural Network (CNN) is a Deep Learning technique employed for the examination and categorization of digital picture data [17] [18]. CNN possesses the benefit of automated feature extraction, as opposed to machine learning which still requires operator intervention [19]. CNN achieves the highest level of accuracy in classifying images [20] [21]. Sarkar did a study utilizing CNN to classify three distinct forms of brain tumors, achieving a high accuracy rate of 91% [22]. In 2014, a novel CNN method was developed to categorize three types of tumors, with a precision rate of 96.56% [23].

Prior studies have shown that the CNN architecture is effective in classifying images. Nevertheless, the CNN architecture faces numerous obstacles. An issue frequently encountered in the training of deep networks is the loss of gradient during the process of backtracking [24]. The training process is impeded by the fact that gradients in CNNs can become exceedingly small when approaching the initial layers [25]. CNNs suffer from the issue that the features acquired by the initial layers are not effectively exploited by the subsequent layers [26]. CNNs often possess a large number of parameters due to the interconnectedness between each layer and all the layers that follow it [27]. Using parameters in this way can be inefficient, particularly in deep models that include numerous layers. Consequently, the implemented model was adjusted to address this issue. In their 2017 study, Huang et al. [28] demonstrated that LeNet CNN fail to fully use the characteristics of preceding neural network layers. Huang et al. introduces a novel DenseNet (Dense Convolutional Network) that effectively utilizes training features.

DenseNet employs direct connections between every pair of layers, enabling gradients to propagate straight to preceding layers with minimal attenuation, hence mitigating the issue of vanishing gradients [29]. In DenseNet, the direct connections between each layer and all the layers above it allow for the direct utilization of information learned by early levels by deeper layers [30]. DenseNet achieves parameter efficiency by recycling features from each layer through direct connections, resulting in a reduction in the number of parameters [31].

The study employed DenseNet121 to categorize three distinct categories of brain tumors: meningioma, glioma, and pituitary. In this study, we enhance the DenseNet121 design by incorporating Dropout and GlobalAveragePooling layers following the last transition layer. The purpose of incorporating this layer is to enhance the representation of features and mitigate the issue of overfitting. Various hyperparameters, such as epoch, optimizer, and activation function, are compared to determine the ideal hyperparameters that result in the maximum level of precision. We will assess the

performance by comparing it with several architectures, including Basic CNN and Basic DenseNet.

MATERIAL AND METHODS

The research methodology initiates with acquiring a brain MRI image dataset, which is subsequently subjected to data processing via resizing the images to dimensions of 240x240. The data that has been processed is divided into two separate datasets: one for training and one for testing. The ratio of the training dataset to the testing dataset is 80:20. Performance, accuracy, precision, recall, and specificity were subsequently computed for the confusion matrix by the DenseNet121 model. Data testing represents the ultimate phase. Refer to Figure 1 for additional information.

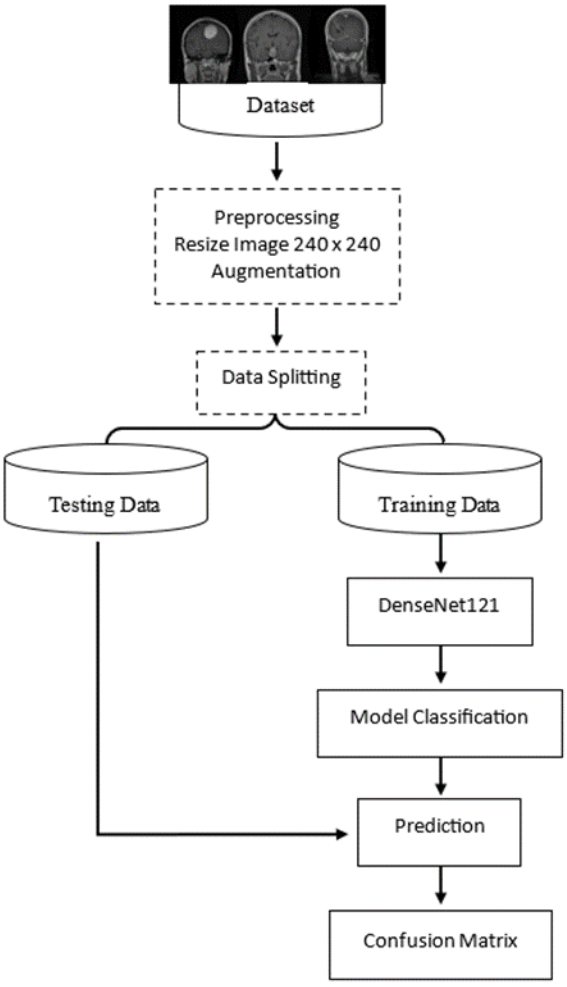

Fig 1. Proposed method

Brain Tumor Dataset

The dataset utilized in this study was collected from the Chandrabhaga Clinic and Nursing Home in 2019. It consisted of 3264 MRI images specifically focused on the brain. The dataset employed in this study was annotated for each class by professionals. The classifications or classes are categorized into three groups: meningioma, pituitary, and glioma.

MRI scans display cross-sectional images in the axial, sagittal, and coronal planes, which are subsequently combined into a single image for each category. The total number of images for Meningioma Tumors was 937, for Pituitary Tumors it was 901, and for Glioma Tumors it was 926. Figure 2 displays an example dataset.

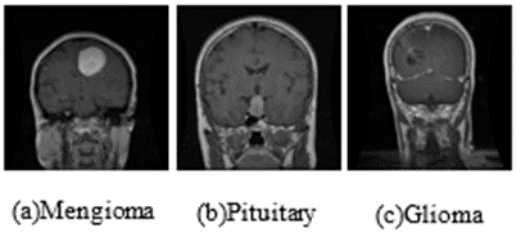

Fig 2. Sample data of brain tumor dataset

DenseNet

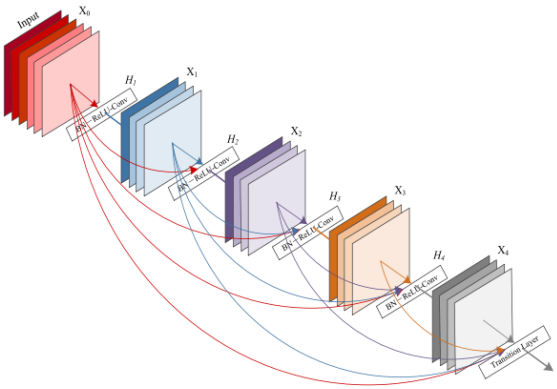

Fig 3. DenseNet architecture [30]

DenseNet is a cutting-edge CNN structure specifically developed for the purpose of detecting visual object. It stands out for its ability to achieve high performance with a reduced number of parameters. The introduction of Densenet was place at the 2017 conference, presented by Huang Go [28]. DenseNet calculates the output l^{th} layer by applying the nonlinear transformation $H_l(.)$ to the output l^{th} layer (X_l) before X_{l-1} in a general manner. Refer to Equation1.

$$X_l = H_l(X_{l-1}) \quad (1)$$

The variable X_{l-1} represents the input from previous layer, whereas H represents the result of a series of computational operations performed in layers, including Batch Normalization (BN), Rectified Linear Unit (ReLU), and convolution (Conv). The output feature maps of layers are combined by DenseNets rather than summarizing them with the input [32]. DenseNet enhances the transmission of information between layers by establishing a streamlined communication architecture. The l^{th} layer is influenced by the input from all preceding layers, incorporating their features. The equation is subsequently converted into equation 2:

$$X_l = H_l[X_0, X_1, X_2, \dots, X_{l-1}] \quad (2)$$

The tensor $[X_0, X_1, X_2, \dots, X_{l-1}]$ represents the output map of the previous layer. After the H_l (.) function, there exists a nonlinear transformation function. The function consists of three main operations: bump normalization (BN), activation using rectified linear units (ReLU), and pooling and convolution (CONV).

Preprocessing

The data is processed and examined for the purpose of categorization. Calculate the quantity of data needed for the data preparation phase, specifically 3264 photographs from three categories: meningioma, pituitary, and glioma.

Oversampling is a technique used to combine many data types in order to achieve a balanced collection of data. This practice is commonly known as data preparation. After achieving data balance, the CNN technique will be utilized to process the data. CNN are a specific form of deep learning methodology. The CNN approach employs a multi-layered processing technique to detect and extract data characteristics.

DenseNet121 Architecture

The optimization of multiple hyperparameters was evaluated to get the optimal parameter combination and achieve high accuracy in the development of the DenseNet121 model, as seen in Table 1. Figure 4 displays the architecture of Modified DenseNet121.

Figure 5(A) displays the Dense block. Each dense block procedure consists of batch normalization, ReLU activation, and convolution with a 1 x 1 filter. This is followed by another operation of ReLU activation and convolution with a 3 x 3 filter, where the matrix values are interconnected. Otherwise, the matrix values should be merged. The purpose of this procedure is to act as a bottleneck, effectively reducing the amount of parameters and computations in the model. The value is multiplied by 24, and the dense 4 block undergoes a convolution process that is multiplied by 16.

The transition layer, depicted in Figure 5(B), is situated between the two compact blocks. During the convolution and pooling process, the feature size undergoes alterations. The transition layer consists of convolution operations using 2 x 2 filters and 1 x 1 average pooling with strides of 2. The DenseNet121 design consists of three transition layers, specifically transition layer 1, transition layer 2, and transition layer 3.

Following that, consist of a Dropout layer and a GlobalAveragePooling2D layer. The purpose of this layer is to compute the mean value of all the feature maps and combine them into a single tensor1D. Next, incorporate the softmax activation function as the final layer of the DenseNet121 model. This layer computes values that are in close proximity to 0, 1, and 2. A value of 0 is used to classify meningioma. Option 1 is used to determine the type of glioma, whereas option 2 is used to determine the type of pituitary tumor.

Training and Testing

During the preparation stage, the input dataset is obtained and resized to dimensions of 224X224. The dataset is partitioned into training and testing data with a ratio of 80:20. The goal of this assessment is to evaluate the performance of the model that will be developed during the pre-training phase. 80% of the training process is focused on leveraging data for training purposes.

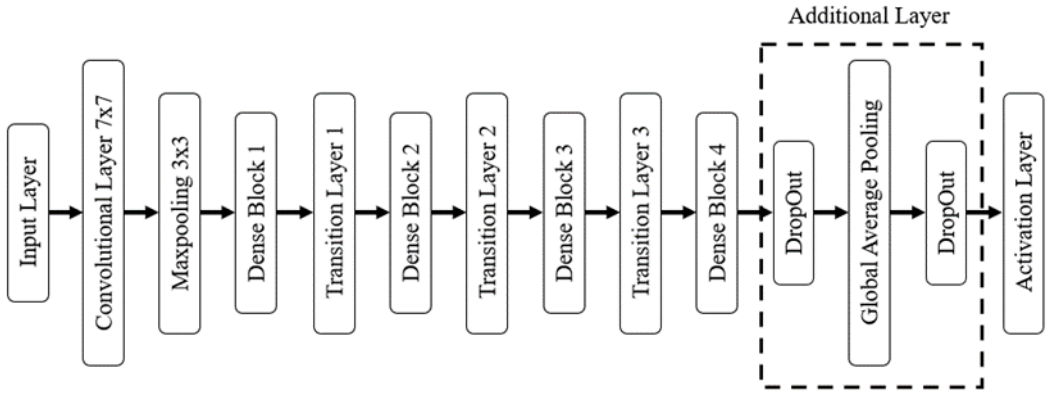

Fig 4. Modified DenseNet121 architecture

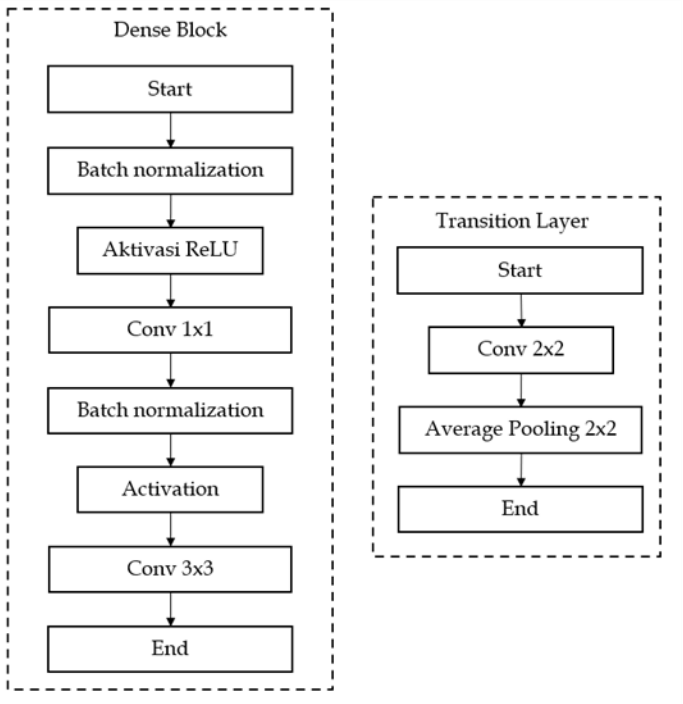

Fig 5. Dense block architecture (A) and transition layer (B)

Table 1. Hyperparameter of Experimental Models

Hyperparameter	Value
Batch size	32, 64, 128
Learning rate	0,001
Optimizer	ADAM, SGD
Activation function	Softmax ReLU
Epoch	50, 100, 150, 200

RESULT AND DISCUSSION

Result

Three distinct networks were chosen for examination using Google Colab to execute the application. The networks included in this set are the Basic CNN, Basic DenseNet, and Modified DenseNet121. A fundamental Convolutional Neural Network (CNN) typically consists of three convolutional layers and two pooling layers. Multiple parameters were modified to determine the potential outcomes that can be achieved by this architecture. An analysis is conducted on the total number of experiments in the system, which consists of 200 epochs, and the corresponding values. The results are presented in table 2.

According to the table, the highest level of accuracy achieved is 84,24%. In order to evaluate limitations on the system, a network is established to utilize test data. While the model achieved a high success rate during training, it was noted that it performed poorly when testing. The testing results are displayed in the confusion matrix depicted in Figure 6(A). The precision, recall, specificity, and F1 score can be computed using the confusion matrix.

In order to conduct a comprehensive evaluation of the model's performance, the value of each tumor class was individually assessed during the testing phase. The meningioma tumor class is denoted as class 0, the glioma tumor is denoted as class 1, and the pituitary tumor is denoted as class 2. Table 5 displays the performance metrics of the simple CNN model throughout the testing phase.

The structure of a classical DenseNet consists of an initial convolution layer followed by maxpooling layers, dense blocks, transition layers, and dense layers. This structure deviates from the fundamental structure of the CNN model. The fundamental densenet layer comprises 189 layers. The objective of comparing the basic densenet with the modified densenet121 is to observe significant alterations in network complexity that surpass those of the suggested model. Similar to the last test case, modifications were made to the hyperparameters in order to ascertain the highest level of accuracy throughout the training phase.

According to the data in table 3, the accuracy of the model has improved in comparison to the prior model. The maximum level of accuracy achieved is 92,29%. The testing phase is conducted in order to generate a confusion matrix show in Figure 6(B). Table 6 displays the test outcomes of the fundamental densenet model.

The Densenet121 modification is implemented in the final experiment. The architecture of this model is altered by incorporating a dropout layer, a 2D global average pooling layer, another dropout layer, and a densenet layer at the conclusion of the structure. This study entailed constructing a DenseNet121 model and adjusting numerous hyperparameters. The experiment yielded the highest training accuracy of 98,24% when employing the proposed model. This outcome is the most elevated compared to previous models. The ADAM optimizer, when used with a learning rate of 0.001, consistently attains the highest degree of accuracy. Table 4 presents a comparison of hyperparameters throughout the training phase.

In the Densenet experiment, two dropout layers were incorporated into the fully linked layer to assess the impact on accuracy. Implemented dropout regularization technique to mitigate the problem of overfitting. The hyperparameters have been defined as follows: 150 epochs, ADAM optimizer, and Softmax activation. Various dropout values ranging from 0.1 to 0.8 will be tested. The findings are displayed in Figure 7. The optimal performance within this range is achieved by utilizing a dropout layer with a rate of 0.8, resulting in an accuracy of 97.82%.

The testing phase is used to assess the model's ability to accurately categorize photos. The peak performance was attained at epoch 150 by utilizing the ADAM optimizer and Softmax Activation Function. Figure 6(C) displays the confusion matrix. According to the confusion matrix, the suggested model demonstrates excellent picture classification capabilities. Table 7 displays the test performance outcomes of the altered densenet121 model.

Table 8 presents a comparative analysis of the mean values for precision, specificity, recall, f1 score, and accuracy for all the models that were tested. Figures 8 and 9 display the training and validation graphs for

both the basic DenseNet model and the suggested model. According to Figure 8, the initial epoch of the basic densenet loss graph shows a sudden increase followed by a drop in the second epoch. When comparing the two illustrations, it is evident that the modified DenseNet121 model outperforms the basic DenseNet model.

Discussion

This study employs the ADAM Optimizer and Stochastic Gradient Descent (SGD) with a learning rate of 0.001. Furthermore, the utilization of a bigger epoch results in increased runtime for each program. The graphs depicted in Figures 8 and 9 demonstrate convergence at epoch 20. There is no necessity to include an additional epoch. The relationship between the time value and the loss value is inversely proportional. Concurrently, the precision value rises in direct correlation with the number of epochs. The experiment is backed by the test results, which demonstrated the maximum level of accuracy, specifically 98.24%, while utilizing the ADAM Optimizer function with Activation softmax, epoch 150, and dropout rate 0,8.

The DenseNet121 design is chosen due to its efficiency in terms of parameter usage and computational requirements, while yet achieving state-of-the-art performance. DenseNet121 exhibits a steady improvement in accuracy as the number of parameters grows, without any indications of performance deterioration or overfitting.

Table 9 presents a juxtaposition of the intended research in this study with past studies on brain tumor classification. According to the comparative table, the Modified DenseNet121 classification model is highly effective in classifying brain cancers. Implementing routing by agreement in CapsNet necessitates a substantial number of iterative procedures [33]. The suggested model employs dense blocks, enabling the reuse of initial features, hence accelerating computation. This also aids in mitigating the issue of vanishing gradients, hence facilitating smoother gradient movement throughout the network. In contrast to Alexnet [34], VGG16 [35], and VGG19 [36], this model has a reduced number of layers and lacks dense layers, rendering it more prone to experiencing disappearing gradients. The incorporation of dropout and GlobalAveragePooling layers in the model helps prevent overfitting.

Figure 10 displays an MRI image of the brain that is recognized as distinct from the original. This is produced by the presence of features that are almost identical between different classes. When various classes exhibit highly similar characteristics, the model may encounter challenges in distinguishing between them. The derived characteristics from the data may lack sufficient discriminative power to differentiate between distinct classes. When the characteristics of two classes exhibit a high degree of similarity or overlap, the model encounters challenges in accurately delineating distinct boundaries between the classes. Certain classes may have highly comparable structures or patterns. For instance, meningiomas and gliomas may exhibit comparable morphological features in MRI imaging, posing a challenge for models to distinguish between them.

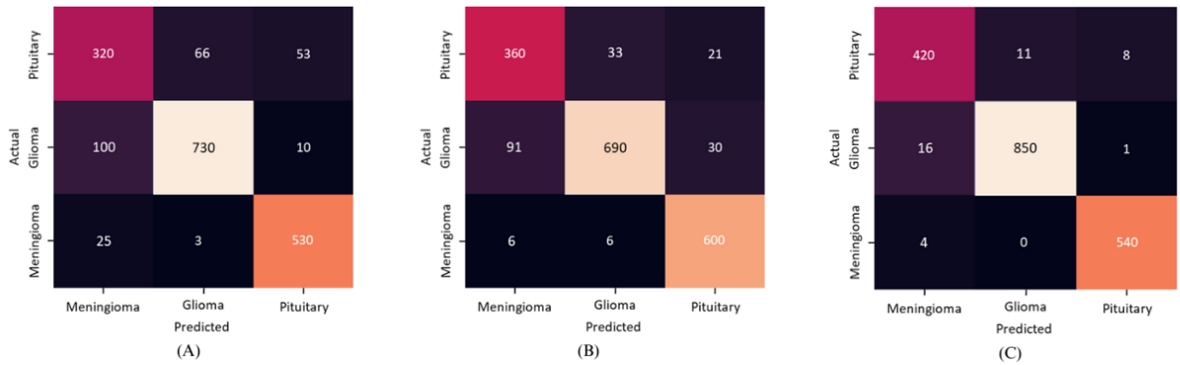

Fig 6. Result of Confusion Matrix Basic CNN (A), Basic DenseNet (B), and Modified DenseNet121 (C)

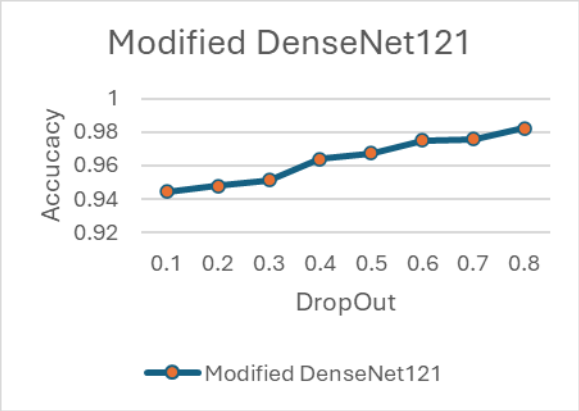

Fig 7. Graph of accuracy results with various levels of dropout rate

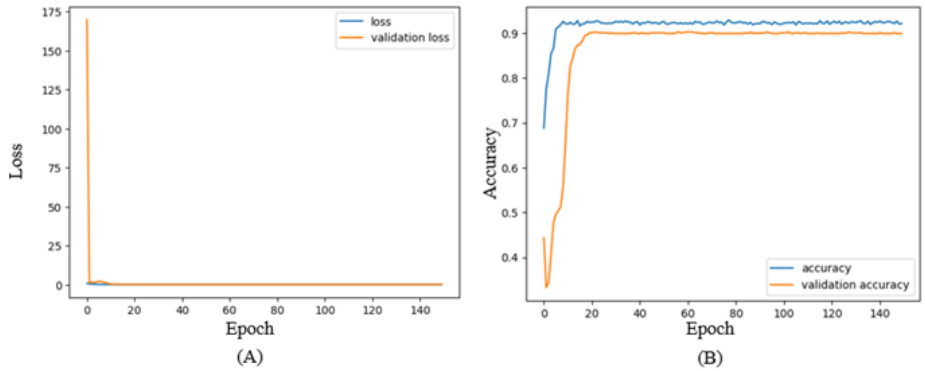

Fig 8. Basic DenseNet model training validation loss and accuracy

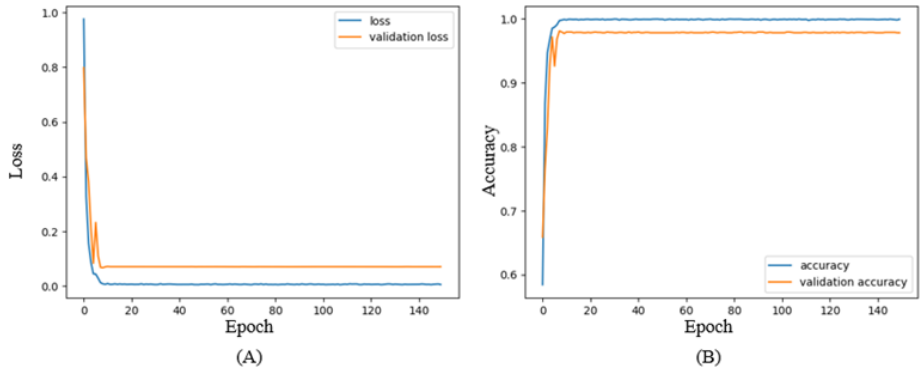

Fig 9. Modified DenseNet121 model training validation loss and accuracy

Fig 10. Examples of misidentified images

Table 2. Values of Basic CNN Architecture Training Stage

Optimizer	Epoch	Accuracy (%)	
		Softmax	ReLU
ADAM	50	83,40	53,28
	100	84,51	54,46
	150	84,24	55,37
	200	86,24	55,37
SGD	50	79,54	46,48
	100	80,26	47,37
	150	80,64	48,96
	200	80,64	48,96

Table 3. Values of Basic DenseNet Architecture Training Stage

Optimizer	Epoch	Accuracy (%)	
		Softmax	ReLU
ADAM	50	92,11	54,49
	100	92,11	55,55
	150	92,29	56,27
	200	92,29	56,34
SGD	50	86,49	48,56
	100	87,68	48,89
	150	88,20	49,34
	200	88,20	49,34

Table 4. Values of Modified DenseNet121 Architecture Training Stage

Optimizer	Epoch	Accuracy (%)	
		Softmax	ReLU
ADAM	50	97,13	60,29
	100	97,47	61,05
	150	98,28	60,65
	200	92,24	60,14
SGD	50	9,88	49,53
	100	92,53	49,75
	150	92,74	50,28
	200	92,74	60,29

Table 5. Performance of the Basic CNN Architecture on the Testing Stage by Class

Basic CNN	Performance (%)				
	Precision	Specivicity	Recall	F1 Score	Accuracy
Meningioma (0)	72,89	91,51	68,81	70,79	86,71
Glioma (1)	86,9	89,4	91,36	89,07	90,25
Pituitary (2)	94,98	94,74	89,37	91,93	93,51

Table 6. Performance of the Basic DenseNet Architecture on the Testing Stage by Class

Basic DenseNet	Performance (%)				
	Precision	Specivicity	Recall	F1 Score	Accuracy
Meningioma (0)	86,95	96,05	76,92	81,62	91,17
Glioma (1)	85,15	89,50	94,65	89,65	91,33
Pituitary (2)	97,80	97,99	93,89	95,80	92,22

Table 7. Performance of the Modified DenseNet121 Architecture on the Testing Stage by Class

Modified DenseNet121	Performance (%)				
	Precision	Specivicity	Recall	F1 Score	Accuracy
Meningioma (0)	95,67	98,65	95,45	95,55	97,89
Glioma (1)	98,01	98,28	98,72	98,36	98,48
Pituitary (2)	99,26	99,68	98,36	98,80	99,28

Table 8. Comparison Table of All Models

Model	Avg Performance (%)				
	Precision	Specivicity	Recall	F1 Score	Accuracy
Basic CNN	84,92	91,88	81,18	83,93	90,15
Basic DenseNet	89,97	94,51	88,48	89,02	91,57
Modified DenseNet 121	97,64	98,87	97,51	97,57	98,55

Table 9. Comparison of Accuracy Performance The Proposed Method and Previous Related

Model	MRI Model	Method	Result
Afshar [29]	T-1	CapsNet	90,89%
Kavin [30]	T-1	AlexNet	92,60%
Sevli [31]	T-1	VGG16	94,42%
Swati [32]	T-1	VGG19	94,82%
Proposed method	T-1	Modified DenseNet121	98,24%

CONCLUSION

Brain tumors are characterized by the unregulated and aberrant proliferation of cells in brain tissue, leading to the disruption of normal brain function. Medical professionals can utilize DenseNet121 to assist in making informed judgments regarding additional treatment options. This design is utilized to assess optimization, epoch, and activation. The optimization algorithms employed are ADAM and SGD. The experiment consisted of four epochs: 50, 100, 150, and 200. The utilized Activation Functions were Rectified Linear Unit (ReLU) and Softmax. The DropOut rate varies between 0,1 and 0,8. The model achieved optimal results using the ADAM optimizer, the softmax activation function, and training for 150 epochs. The DropOut rate that yields the highest performance 0,8.

To advance research, it is crucial to classify healthy brains and enhance the precision of models by employing alternative architectures that may effectively utilize superior feature extraction techniques. In addition, it can also leverage architectures that offer accurate class label prediction performance, such as Support Vector Machines (SVM) and Extreme Gradient Boosting (XGBoost).

ACKNOWLEDGEMENTS

This research has been supported trough Directorate General of Higher Education, Ministry of Education and Culture of the Republic of Indonesia (DRTPM) under the Basic Fundamental Research Scheme.

REFERENCES

[1] R. Azzarelli, B. D. Simons, and A. Philpott, "The developmental origin of brain tumours: A cellular and molecular framework," *Development (Cambridge)*, vol. 145, no. 10. Company of Biologists Ltd, May 01, 2018. doi: 10.1242/dev.162693.

[2] M. M. Badža and M. C. Barjaktarović, "Classification of brain tumors from mri images using a convolutional neural network," *Applied Sciences (Switzerland)*, vol. 10, no. 6, Mar. 2020, doi: 10.3390/app10061999.

[3] J. Kang, Z. Ullah, and J. Gwak, "Mri-based brain tumor classification using ensemble of deep features and machine learning classifiers," *Sensors*, vol. 21, no. 6, pp. 1–21, Mar. 2021, doi: 10.3390/s21062222.

[4] A. Kadam, S. Bhuvaji, and S. Deshpande, "Brain Tumor Classification using Deep Learning Algorithms," 2021. [Online]. Available: www.ijraset.com

[5] H. Sung *et al.*, "Global Cancer Statistics 2020: GLOBOCAN Estimates of Incidence and Mortality Worldwide for 36

[6] J. Amin, M. Sharif, M. Yasmin, and S. L. Fernandes, "A distinctive approach in brain tumor detection and classification using MRI," *Pattern Recognit Lett*, vol. 139, pp. 118–127, Nov. 2020, doi: 10.1016/j.patrec.2017.10.036.

[7] P. K. Chahal, S. Pandey, and S. Goel, "A survey on brain tumor detection techniques for MR images," *Multimed Tools Appl*, vol. 79, no. 29–30, pp. 21771–21814, Aug. 2020, doi: 10.1007/s11042-020-08898-3.

[8] M. K. Abd-Ellah, A. I. Awad, A. A. M. Khalaf, and H. F. A. Hamed, "A review on brain tumor diagnosis from MRI images: Practical implications, key achievements, and lessons learned," *Magnetic Resonance Imaging*, vol. 61. Elsevier Inc., pp. 300–318, Sep. 01, 2019. doi: 10.1016/j.mri.2019.05.028.

[9] H. A. Khan, W. Jue, M. Mushtaq, and M. U. Mushtaq, "Brain tumor classification in MRI image using convolutional neural network," *Mathematical Biosciences and Engineering*, vol. 17, no. 5, pp. 6203–6216, 2020, doi: 10.3934/MBE.2020328.

[10] W. L. Bi *et al.*, "Artificial intelligence in cancer imaging: Clinical challenges and applications," *CA Cancer J Clin*, vol. 69, no. 2, pp. 127–157, Mar. 2019, doi: 10.3322/caac.21552.

[11] E. D. Bander *et al.*, "Tubular brain tumor biopsy improves diagnostic yield for subcortical lesions," *J Neurooncol*, vol. 141, no. 1, pp. 121–129, Jan. 2019, doi: 10.1007/s11060-018-03014-w.

[12] S. Iqbal, M. U. G. Khan, T. Saba, and A. Rehman, "Computer-assisted brain tumor type discrimination using magnetic resonance imaging features," *Biomedical Engineering Letters*, vol. 8, no. 1. Springer Verlag, pp. 5–28, Feb. 01, 2019. doi: 10.1007/s13534-017-0050-3.

[13] R. Vankdothu and M. A. Hameed, "Brain tumor MRI images identification and classification based on the recurrent convolutional neural network," *Measurement: Sensors*, vol. 24, Dec. 2022, doi: 10.1016/j.measen.2022.100412.

[14] N. Vani, A. Sowmya, and N. Jayamma, "Brain Tumor Classification using Support Vector Machine," *International Research Journal of Engineering and Technology*, vol. 4, no. 07, pp. 1724–1729, 2017, [Online]. Available: www.irjet.net

[15] H. T. Zaw, N. Maneerat, and Y. K. Win, *Brain tumor detection based on Naïve Bayes Classification*, vol. 19. 2019.

[16] G. Bekoulis, J. Deleu, T. Demeester, and C. Develder, "Joint entity recognition and relation extraction as a multi-head selection problem," *Expert System with Applications*, vol. 114, no. 30, pp. 34–45, Apr. 2019, doi: 10.1016/j.eswa.2018.07.032.

[17] I. Fahruzi, "SLEEP DISORDER IDENTIFICATION FROM SINGLE LEAD ECG BY IMPROVING HYPERPARAMETERS OF 1D-CNN," *Jurnal Ilmiah KURSOR*, vol. 11, no. 4, pp. 157–164, 2022.

[18] W. Rawat and Z. Wang, "Deep Convolutional Neural Networks for Image Classification: A Comprehensive Review," *Neural Computation*, vol. 29, no. 9. MIT Press Journals, pp. 2352–2449, Sep. 01, 2017. doi: 10.1162/NECO_a_00990.

[19] H. Basri, I. Syarif, S. Sukaridhoto, and M. F. Falah, "INTELLIGENT SYSTEM FOR AUTOMATIC CLASSIFICATION OF FRUIT DEFECT USING FASTER REGION-BASED CONVOLUTIONAL NEURAL NETWORK (FASTER R-CNN)," *Jurnal Ilmiah KURSOR*, vol. 10, no. 1, pp. 1–12, 2019.

[20] R. Anantama, H. Suyono, and M. Aswin, "APPLICATION OF COST-SENSITIVE CONVOLUTIONAL NEURAL NETWORK FOR PNEUMONIA DETECTION," *Jurnal Ilmiah KURSOR*, vol. 11, no. 3, pp. 101–108, 2022.

[21] O. N. Belaid and M. Loudini, "Classification of brain tumor by combination of pre-trained VGG16 CNN," *Journal of Information Technology Management*, vol. 12, no. 2, pp. 13–25, 2020, doi: 10.22059/JITM.2020.75788.

[22] S. Sarkar, A. Kumar, S. Aich, S. Chakraborty, J.-S. Sim, and H.-C. Kim, "A CNN based Approach for the Detection of Brain Tumor Using MRI Scans," *Test Engineering and Management*, vol. 83, pp. 16580–16586, 2020, [Online]. Available: https://www.researchgate.net/publication/342048436

[23] W. Ayadi, W. Elhamzi, I. Charfi, and M. Atri, "Deep CNN for Brain Tumor Classification," *Neural Process Lett*, vol.

53, no. 1, pp. 671–700, Feb. 2021, doi: 10.1007/s11063-020-10398-2.

[24] Q. Zhu, B. Du, B. Turkbey, P. L. . Choyke, and P. Yan, "Deeply-Supervised CNN for Prostate Segmentation," *2017 International Joint Coference on Neural Network (IJCNN)*, pp. 178–184, Mar. 2017, [Online]. Available: http://arxiv.org/abs/1703.07523

[25] F. Badri, M. Taqijuddin Alawiy, and E. M. Yuniarno, "DEEP LEARNING ARCHITECTURE BASED ON CONVOLUTIONAL NEURAL NETWORK (CNN) ON ANIMAL IMAGE CLASSIFICATION," *Jurnal Ilmiah KURSOR*, vol. 12, no. 2, pp. 83–92, 2023.

[26] Md. A. Hossain and Md. S. Alam Sajib, "Classification of Image using Convolutional Neural Network (CNN)," *Global Journal of Computer Science and Technology*, pp. 13–18, May 2019, doi: 10.34257/gjcstdvol19is2pg13.

[27] M. Jogin, Mohana, M. S. Madhulika, G. D. Divya, R. K. Meghana, and S. Apoorva, "Feature extraction using convolution neural networks (CNN) and deep learning," in *2019 3rd IEEE International Conference on Recent Trends in Electronics, Information and Communication Technology, RTEICT 2019 - Proceedings*, Institute of Electrical and Electronics Engineers Inc., May 2019, pp. 2319–2323. doi: 10.1109/RTEICT42901.2018.9012507.

[28] G. Huang, Z. Liu, L. Van Der Maaten, and K. Q. Weinberger, "Densely Connected Convolutional Networks," 2021. [Online]. Available: https://github.com/liuzhuang13/DenseNet.

[29] G. Huang, Z. Liu, L. Van Der Maaten, and K. Q. Weinberger, "Densely Connected Convolutional Networks," 2017. [Online]. Available: https://github.com/liuzhuang13/DenseNet.

[30] W. Guo, Z. Xu, and H. Zhang, "Interstitial lung disease classification using improved DenseNet," *Multimed Tools Appl*, vol. 78, no. 21, pp. 30615–30626, Nov. 2019, doi: 10.1007/s11042-018-6535-y.

[31] N. HASAN, Y. BAO, A. SHAWON, AND Y. HUANG, "DENSENET CONVOLUTIONAL NEURAL NETWORKS APPLICATION FOR PREDICTING COVID-19 USING CT IMAGE," *SN COMPUT SCI*, VOL. 2, NO. 5, SEP. 2021, DOI: 10.1007/S42979-021-00782-7.

[32] A. Gajre, O. S. Khaladkar, and A. J. Patil, "DenseNet for Brain Tumor Classification in MRI Images," 2022. [Online]. Available: www.ijisrt.com

[33] P. Afshar, K. N. Plataniotis, and A. Mohammadi, "Capsule Networks for Brain Tumor Classification based on MRI Images and Course Tumor Boundaries," pp. 1368–1372, Nov. 2019, [Online]. Available: http://arxiv.org/abs/1811.00597

[34] K. Kavin Kumar *et al.*, "Brain Tumor Identification Using Data Augmentation and Transfer Learning Approach," *Computer Systems Science and Engineering*, vol. 46, no. 2, pp. 1845–1861, 2023, doi: 10.32604/csse.2023.033927.

[35] O. Sevli, "Performance Comparison of Different Pre-Trained Deep Learning Models in Classifying Brain MRI Images," *Acta Infologica*, vol. 5, no. 1, pp. 141–154, Jul. 2021, doi: 10.26650/acin.880918.

[36] Z. N. K. SWATI *ET AL.*, "BRAIN TUMOR CLASSIFICATION FOR MR IMAGES USING TRANSFER LEARNING AND FINE-TUNING," *COMPUTERIZED MEDICAL IMAGING AND GRAPHICS*, VOL. 75, PP. 34–46, JUL. 2019, DOI: 10.1016/J.COMPMEDIMAG.2019.05.001